DINAME 2017 - Proceedings of the XVII International Symposium on Dynamic Problems of Mechanics
A. T. Fleury, D. A. Rade, P. R. G. Kurka (Editors), ABCM, São Sebastião, SP, Brazil, March 5-10, 2017

Experimental Assessments of the Added Mass of Flexible Cylinders in Water: the Role of Modal Shape Representation

Rafael Salles[1], **Celso Pupo Pesce**[1]

[1] Offshore Mechanics Laboratory, Escola Politécnica, University of São Paulo, rafael.salles@usp.br, ceppesce@usp.br

Abstract: A flexible vertical cylinder model, fixed at both ends, is tested experimentally immersed in water and then in air. Galerkin's decomposition is applied to obtain a Reduced Order Model (ROM) from a continuum one. Two closed-form trial modal shapes are chosen for the modal decomposition process. Then, modal added mass is assessed using classical Fourier and Hilbert transform (HT) signal analyses, comparing the model eigenvalues with the frequency evaluated from the experimental signals. The choice of modal shape is shown to alter significantly added mass experimental assessment. Similarity to classic results with rigid cylinders is achieved by taking a sufficiently proper modal representation. Moreover, the first mode added mass coefficient attains the same value of that previously determined for a cantilevered flexible circular cylinder, by Pesce and Fujarra (2000).

Keywords: Modal Decomposition, Added Mass, Flow Induced Vibration, Flexible Cylinder

NOMENCLATURE

Latin symbols

a: added mass coefficient, $a = m_a/m_s$
A: modal amplitude
C_a: added mass coefficient, $C_a = m_a/m_d$
$\hat{C}_a$: 'potential-flow' added mass coefficient, $\hat{C}_a \approx 1$
C_D: drag force coefficient
C^h: modal drag force coefficient
C_m: inertia coefficient, $C_m = 1 + C_a$
c_s: linear viscous damping coefficient
C^s: modal linear viscous damping coefficient
D: diameter
EA: axial stiffness
EI: bending stiffness
f_d: damped natural frequency (measured)
$\hat{f}_n$: natural frequency (calculated)
k: mode number
K, KC: Keulegan-Carpenter number
L: stretched length
L_0: unstretched length
L_i: immersed length
L_t: total length
M: modal mass m_a: additional mass
M_a: modal added mass
M_d: modal displaced mass
m_s: structural mass per unit length
M_s: modal structural mass
$m^\star$: reduced mass parameter
$m_1^\star$: first mode reduced mass
N_b: equivalent normal traction
$N_{b(0)}$: traction at the cylinder bottom
Re: Reynolds number
t: time
$T(z,t)$: tension
$\mathbf{u}(z,t)$: displacement vector
U_m: mean velocity

Greek symbols

$\underline{\alpha}$: *quasi*-Bessel mode parameter
β: Sarpykaya's β–parameter
$\underline{\beta}$: *quasi*-Bessel mode wave number
$\bar{\gamma}$: linear weight
γ_i: immersed linear weight
η: modal rigidity
ζ: linear viscous damping coefficient
ν: kinematic viscosity
ξ: dimensionless modal amplitude
ρ_w: water specific mass
ψ: modal shape
ω: angular frequency

Subscripts

I: relative to the reduced mass case I
II: relative to the reduced mass case II
a: relative to experiment in air
d: natural damped
j: relative to the j-th mode
k: relative to the k-th mode
n: natural non-damped
w: relative to experiment in water
y,z: relative to Cartesian coordinates

INTRODUCTION

Oil and gas exploitation has been a major world economic activity, over the years. In the offshore activities scenario, risers – long tubular structures connecting the floating unity to the sea bed – play important roles in drilling, prospection and transport of those commodities. Flexible vertical risers are commonly used in offshore operations and they are subjected to hydrodynamic loads due to current, Vortex Induced Vibration (VIV), as well as parametric and internal resonance caused by movements imposed at the top by the floating unit vessel; see Fig. 1a. The dynamics of such structures is usually assessed through nonlinear analytical and numerical models, which are commonly validated with laboratorial experiments, carried out on small scale physical models.

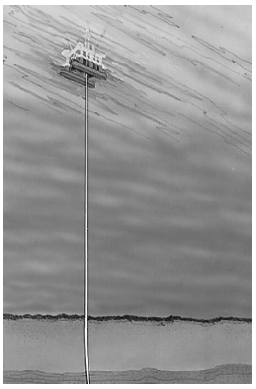

(a) Vertical riser schematic installation in a floating unit vessel. Adapted from Kuiper (2008).

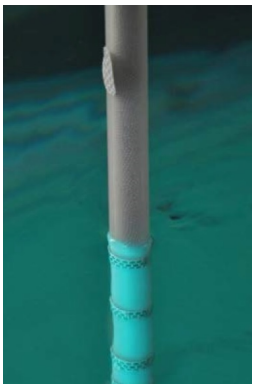

(b) Experimental model of flexible vertical cylinder in a towing tank. Extracted from Salles (2016).

Figure 1 – Vertical riser schematic representation and vertical flexible cylinder scaled model

On this road, by using an optical tracking system (Qualisys™), composed by underwater and aerial cameras, experimental tests conducted with a flexible vertical cylinder in water were carried out; Pesce (2013). Through a Galerkin's modal decomposition scheme, assuming a simple sinusoidal mdal shape representation, parametric resonances excited by the periodic variation of tension were addressed; see Franzini *et al.* (2015).

Such a simple choice regarding modal shapes was also followed in Fu et al (2014) and in Franzini et al (2016a,b), analysing the behavior of long flexible cylinder subjected to hydrodynamic loads. Thorsen *et al.* (2016) proposed a semi-empirical numerical VIV model, verifying their calibrated coefficients by comparing the numerical results with the experimental data obtained in Fu *et al.* (2014). However, neither Franzini *et al.* (2015), Fu *et al.* (2014) or Thorsen *et al.* (2016) assessed the modal added mass parameter, restricting themselves to adopting the potential flow asymptotic limit, $\hat{C}_a = 1$, for all modes. As a matter of fact, a first assessment on the influence of drag and added mass coefficients on the response of a parametrically excited vertical flexible cylinder was made by Franzini *et al.* (2016), through a parametric study with a nonlinear reduced order model. Nonetheless, fundamental studies on modal added mass of flexible cylinders are not commonly found in the technical literature. A single experimental assessment is reported in Pesce and Fujarra (2000), concerning the first vibration mode of a cantilevered flexible cylinder, where $C_{a,1} = 1.17$ is obtained. This is not the case for rigid cylinders. Early in the '70s, Sarpkaya (1977) provided an extensive experimental study on rigid cylinders subjected to oscillatory flows, aiming at a better evaluation of hydrodynamics coefficients, as drag and inertia parameters, for a large range of Reynolds (Re) and Keulegan-Carpenter (KC) numbers. Sarpkaya (1977) experimentally showed that, for low KC, the inertia coefficient tends to the expected asymptotic value $C_m = 1 + C_a \approx 2$, in which $\hat{C}_a \approx 1$ is the potential flow added mass coefficient of a rigid cylinder; see Fig. 2.

Recently, Salles (2016) assessed the modal added mass coefficient of a vertical flexible cylinder using the same experimental data base used in Franzini *et al.* (2015). Salles used sinusoidal modes and obtained values of added mass coefficients larger than $C_a = 1$.

The present study aims at identifying the role modal shape representation could play on the assessment of the corresponding added mass coefficient. Taking sinusoidal or 'quasi-Bessel' modes in Galerkin's projection, modal added mass coefficients are evaluated and compared. The results are interpreted on the light of Sarpkaya's (1977) rigid cylinders experimental results, contributing to the discussion on the ad hoc assumption, $C_a = 1$, usually taken by many authors when dealing with vibrations of flexible cylinders in water.

Sarpkaya's (1977) experiments on added mass of a rigid cylinder under oscillatory flow

One of the main points of riser dynamics modeling is the correct evaluation of hydrodynamic forces. In particular, inertial and viscous forces. The wellknown concepts of 'added mass' and 'damping' play then a role of paramount importance.

The classic work by Sarpkaya (1977), with a rigid cylinder under oscillatory flow, brings quite comprehensive results about the inertia coefficient, $C_m = 1 + C_a$ – where $C_a = ms/m_d$, being m_a the added mass and m_d the displaced mass, both per unit length –, related to two important parameters: the Keulegan–Carpenter number $KC = K = \frac{UmT}{D} \approx 2\pi\frac{A}{D}$, and the Reynolds number, $Re = \frac{UmD}{\nu}$ or the β-parameter, $\beta = \frac{Re}{K}$. For the non specialized reader, one of the seminal results from Sarpkaya's extensive experimental study is summarized in Fig. 2, where the small amplitude asymptotic limit for the inertia coefficient is recovered as $C_m \to 2^+$. For flexible circular cylinders, however, no extensive and comprehensive parallel study may be found in the technical literature, at least to the authors' knowledge.

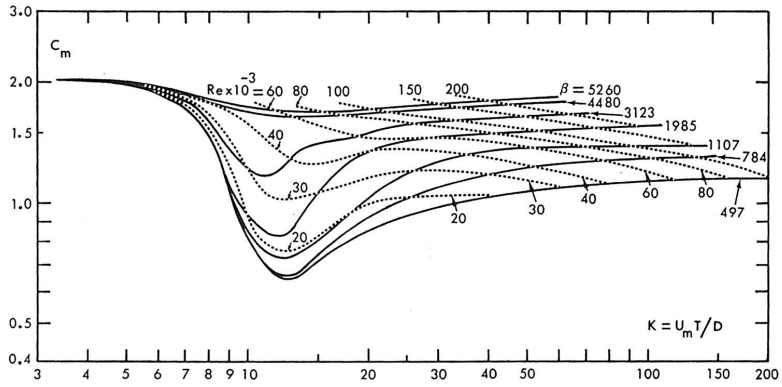

Figure 2 – Inertia coefficients, $C_m = C_a + 1$, for a rigid circular cylinder as function of Keulegan–Carpenter number, K. Extracted from Sarpkaya (1977).

The vertical flexible cylinder experimental set up

In the core of an extensive research project on nonlinear dynamics of risers, a small scale model was designed and built as a flexible cylinder, under proper similarity laws. The Froude scale was used as the leading similarity law, as offshore structures are subjected to loads arising from the floating unit vessel motions, mainly caused by the action of free surface waves.

Pereira *et al.* (2012) presented a study of how the similitude parameters were chosen, leading to the construction of a small-scale model made from a silicon tube filled with stainless steel micro-spheres; see Fig. 1b. In the small scaling methodology, within a large set of dimensionless parameters, geometric rigidity (tensioning), axial stiffness, bending stiffness, immersed weight and added mass play dominant roles. See also Pereira (2014) and Salles (2016).

An optical tracking system composed by aerial and submerged infrared cameras was used to measure cartesian coordinates of reflective targets placed all along the model length. This measurement technique is non invasive, cleaner and easier to be implemented, compared to traditional ones, which use strain gages and/or accelerometers; see, *e.g.*, Pesce and Fujarra (2000); Morooka and Tsukada (2013). The small model elastica may then be reconstructed at any instant of time from the tracked targets. A load cell was installed at the top of the model to register tension. The bottom and top extremities are fixed in the supporting structure.

The experimental set up was designed for a comprehensive series of tests, carried out at IPT towing tank; see Fig. 3a. Such tests involved three kinds of excitation loadings (see Pesce (2013)): (i) periodic vertical displacement imposed at the top; (ii) relative constant current profile, by the towing carriage; (iii) combining (i) and (ii). For an extensive report on the main experimental results, see Franzini *et al.* (2015) and Franzini *et al.* (2016a,b), Pereira *et al.* (2016).

All those experiments were preceded by decaying tests in water, in order to assess natural frequencies, damping and, focus of the present analysis, added mass coefficients.

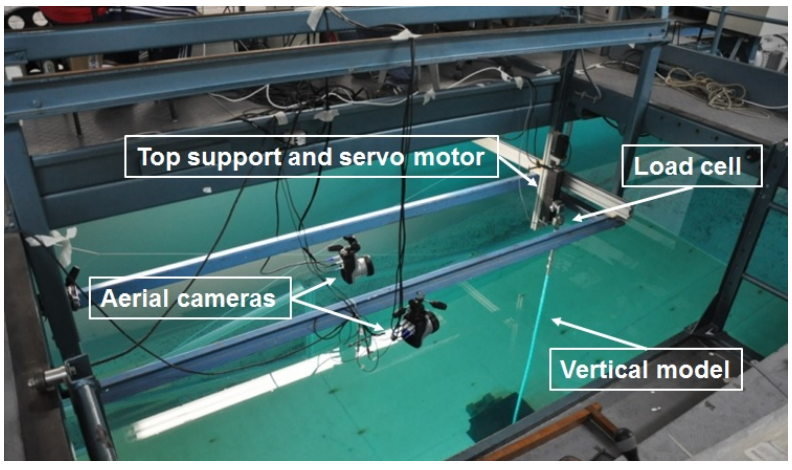

(a) Experimental set up of the flexible vertical cylinder in water. Extracted from Salles (2016).

(b) Experimental set up of the flexible cylinder in air. Extracted from Salles (2016).

Figure 3 – Vertical flexible cylinder scaled model: experimental campaigns in water and in air.

For such an assesment, another experimental campaign was performed outside the towing tank. The experimental tests in air, see Fig. 3b, were carried out in order to obtain a complete structural characterization, disregarding the effects of added mass and drag included in the experimental campaign in water. By comparing decaying tests in air and in water,

added mass and hydrodynamic damping can be assessed, as shown below, essentially following a methodology used in Pesce and Fujarra (2000).

The experiments in air were done with the same small scale riser model used in water. A vertical configuration in air was established, making sure that a first modal rigidity estimation – using a vertical bi-suported heavy ideal string together with trigonometric *Eigenfunctions*, see Salles (2016) – is dynamically equivalent to the value measured in water, where buoyance forces take place. Table 1 presents the physical properties of the aforementioned experimental models, as built.

Table 1 – Model physical properties for both free-decay experimental tests in air and water, as built

Properties		Value	
		Air	**Water**
Unstretched length, L_0	(m)	2.613	2.552
Stretched length, L	(m)	2.665	2.602
Immersed length, L_i	(m)	–	2.257
Diameter, D	(mm)	22.2	
Linear mass, m_s	(kg/m)	1.14	1.19
Linear weight, γ	(N/m)	11.13	–
Immersed linear weight, γ_i	(N/m)	–	7.87
Static tension at the top, T_t	(N)	47.56	40
Axial stiffness, EA	(N)	1200	
Bending stiffness, EI	(Nm^2)	0.056	

MODAL DECOMPOSITION: GALERKIN'S METHOD

Considering an Euler-Beam model as in, Eq. 1, it is possible to use standard Galerkin's decomposition techniques in order to represent the structure dynamics as a sum of a finite mode numbers. The called modes, or *Eigenfunctions* – ψ_k, are smooth functions that do not violate any kinematic system constrain. Notice that hydrodynamic drag forces are essentially nonlinear, though.

$$m_s\frac{\partial^2\mathbf{u}}{\partial t^2}+EI\frac{\partial^4\mathbf{u}}{\partial z^4}+c_s\frac{\partial\mathbf{u}}{\partial t}=\frac{\partial}{\partial z}\left(T\left(z,t\right)\frac{\partial\mathbf{u}}{\partial z}\right)-m_a\frac{\partial^2\mathbf{u}}{\partial t^2}-\frac{1}{2}\rho_w DC_D\left\|\frac{\partial\mathbf{u}}{\partial t}\right\|\frac{\partial\mathbf{u}}{\partial t} \tag{1}$$

For the ideal vertical heavy string, the kinematic system constrains are simply written as $\mathbf{u}\left(0\right)=\mathbf{u}\left(L\right)=\mathbf{0}$, since bending effects are non existent. In such idealized case, where transversal rigidity is due only to tension, Bessel functions of first and second kinds of zeroth order are shown to form the eigenfunctions set; see Pesce *et al.* (1999). Usually, for long beams, geometrical rigidity dominates bending effects, which are relevant just in the neighborhood of the constraints or for higher vibration modes.

A wise integral averaging technique applied by Mazzilli *et al.* (2014) takes bending effects into account through the definition of an additional equivalent tension. Such a technique gives rise to analytical representations for the *Eigenmodes* which are called by the authors '*quasi*-Bessel' modes. Those *Eigenmodes* are used in the present paper. They resemble a closed form WKB solution given in Pesce *et al.* (1999) where extensibility and bending stiffness are disregarded for a catenary shape.

Sinusoidal functions can be used as the simplest 'trial functions' instead, what is also done in the present paper, as a first approximation. See also Franzini *et al.* (2015), Franzini *et al.* (2016c) or Salles (2016) for additional considerations.

Equation 1 is rewritten as Eq. 2, in which an alternative form for the added mass coefficient, $a=m_a/m_s$, is introduced. The non-linear model presented in Eqs. 1–2 considers the effect of flexural rigidity (EI), structural damping (considered to be viscous linear, c_s), the variation of geometric stiffness due to the traction along the model spanwise ($T\left(z,t\right)=T\left(L\right)-\gamma(L-z)$), added inertia ($m_a$) and drag force (considered to be quadratic in the relative velocity with respect to the flow, as in Morison's formula, being C_D the drag coefficient).

$$m_s\left(1+a\right)\frac{\partial^2\mathbf{u}}{\partial t^2}+EI\frac{\partial^4\mathbf{u}}{\partial z^4}+c_s\frac{\partial\mathbf{u}}{\partial t}+\frac{1}{2}\rho_w DC_D\left\|\frac{\partial\mathbf{u}}{\partial t}\right\|\frac{\partial\mathbf{u}}{\partial t}-\frac{\partial T}{\partial z}\frac{\partial\mathbf{u}}{\partial z}-T\frac{\partial^2\mathbf{u}}{\partial z^2}=\mathbf{0} \tag{2}$$

The next step is to obtain a Reduced-Order Model (ROM) from Eq. 2, using Galerkin's method, through a classic separation of variable procedure,

$$\mathbf{u}\left(z,t\right)\approx A^k\left(t\right)\psi_k\left(z\right),\ \text{in which}\ \ \left(i,k\right)\in\mathbb{N}^*\times\mathbb{N}^* \tag{3}$$

where summation is implied. Proceeding with the Galerkin's projection, the dynamic equations can be written:

$$M_{kj}\ddot{A}^k+C^s_{kj}\dot{A}^k+C^h_{kj}\left\|\dot{A}^k\right\|\dot{A}^k+\eta_{kj}A^k=0 \tag{4}$$

in which:

$$M_{kj} = m_s\left(1+a_k\right)\int_0^L \psi_k \psi_j dz$$
$$C^s_{kj} = c_s \int_0^L \psi_k \psi_j dz$$
$$C^h_{kj} = \frac{1}{2}\rho_w D C_D \int_0^L \psi_k \left\|\psi_k\right\| \psi_j dz$$
$$\eta_{kj} = -\int_0^L \left(T'\psi'_k\psi_j + T\psi''_k\psi_j - EI\psi^{IV}_k\psi_j\right)dz$$

Assuming orthogonality conditions to hold[1], non damped and damped natural frequencies would then be given by,

$$\omega_{n,k} = 2\pi f_{n,k} = \sqrt{\frac{\eta_{kk}}{M_{kk}}} \tag{5}$$

and

$$\omega_{d,k} = 2\pi f_{d,k} = \sqrt{1-\zeta^2_{kk}}\,\omega_{n,k}, \text{ in which } \zeta_k = \frac{C^s_{kk}}{2M_{kk}\omega_{n,k}} \tag{6}$$

Modal Basis Representation

As aforementioned, the main criterion to define a function as an approximation for an *Eigenfunction* is to respect all system kinematic constrains. For the flexible cylinder, the system constrains are simply $\mathbf{u}\left(0\right) = \mathbf{u}\left(L\right) = \mathbf{0}$, which could be written as $\psi_k\left(0\right) = \psi_k\left(L\right) = 0$ for every $k \in \mathbb{N}^*$. Mainly, the present work aims to assess how the choice of the projection basis would affect the assessment of the added mass coefficient.

The first basis considered is the exact solution of the classical tensioned string problem, in the absence of a graviational force field. Known as the Pythagorean harmonics of a string, the *Eigenfunctions* are trigonometric as defined in Eq. 7. Hereinafter, the trigonometric modes will form a basis called *Sinusoidal* in the following figures and tables.

$$\psi_k\left(z\right) = \sin\left(k\pi\frac{z}{L}\right) \tag{7}$$

The second basis is formed by *quasi*-Bessel modes presented in Mazzilli *et al.* (2014) and determined from a Timoshenko's beam with non-linearities after an integral averaging process, the flexural stiffness effect being transformed into an equivalent traction, thus reducing the order of the partial differential equation in space, from fourth to second. Such a procedure arrives at an equivalent vertical heavy string problem, which has Bessel's functions as *Eigenfunctions*. By means of an asymptotic approximation, Mazzilli *et al.* reached a closed-form solution, Eq. 8, which also resembles the WKB boundary layer result obtained by Pesce *et al.* (1999).

$$\psi_k\left(z,\eta_k\right) = \frac{1}{\sqrt[4]{1+\underline{\alpha}z}}\sin\left[\underline{\beta}\left(\sqrt{1+\underline{\alpha}z}-1\right)\right] \tag{8}$$

in which:

$$\underline{\alpha} = \frac{\gamma}{N_{bk}}$$
$$N_{bk} = N_{b(0)} + \left(\frac{k\pi}{L}\right)^2 EI\left(1+\frac{3}{16}\xi^2_k\right)$$
$$N_{b(0)} = \frac{EA\left(L-L_0\right)}{L_0}$$
$$\underline{\beta} = \frac{k\pi}{\sqrt{1+\underline{\alpha}L}-1}$$

Henceforward, the *quasi*-Bessel modes will be also called Bessel-like modes. In the present work, Bessel-like modes, *i.e.*, $\xi_k = 0$, were used for the analysis, as vibration amplitude is very small and would not affect the modal representation.

[1] *Quasi*-Bessel, or Bessel-like, modes are non-orthogonal to each other. A orthogonalization procedure is then needed.

Figure 4 shows the first three modes for the Sinusoidal and Bessel-like basis normalized to have its maximum at 1. The solid lines represent the Bessel-like modes and the dashed lines the sinusoidal ones. The Bessel-like modes are more representative of the flexible vertical heavy string. In fact, their maxima occur inside the half lower part, as it would be expected from the analytical solution of the ideal bi-articulated vertical heavy string, the Bessel *Eigenfunctions*.

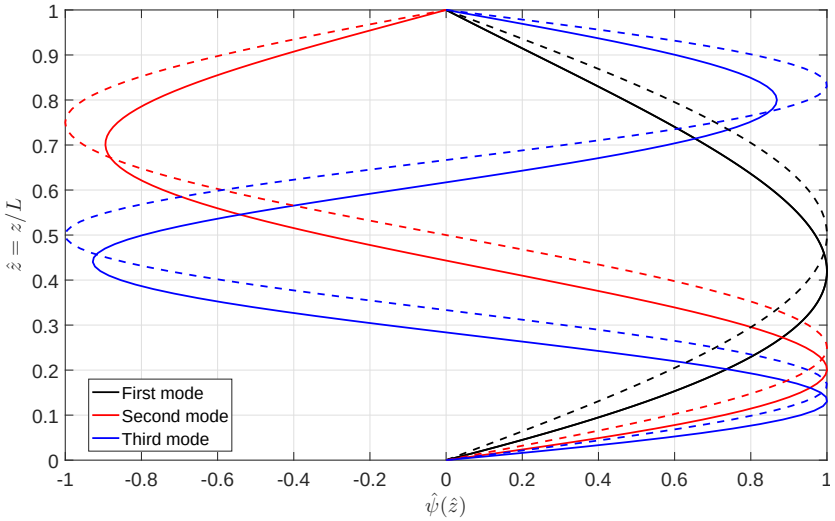

Figure 4 – Graphical representation of the first three sinusoidal (dashed lines) and orthogonalized *quasi*-Bessel modes (solid lines).

Hereafter, only the first mode will be addressed, so that a orthogonalization procedure for the Bessel-like modes may be abandomned in the Galerkin's projection.

ANALYSIS

The modal decomposition is performed using both trigonometric and *quasi*-Bessel fundamental modes. The first (fundamental) mode amplitude series for both decompositions are presented in Figs. 5–8. Notice that time scales are quite different, as decaying in air is much slower than in water.

It is interesting to give the reader some details on the methodology behind the modal analysis adopted. Figure 5 shows the full free-decay amplitude time series upon which the Hilbert Transform (HT) was used in order to determine the signal envelope amplitude. The HT envelope amplitude is then applied to determine the linear viscous equivalent structural damping and to study the instant damped frequency. Figure 5 also shows that there is a time interval chosen for the analysis, marked in red color.

Besides the HT procedure, a standard Fourier (FFT) analysis was carried out, in order to directly assess the damped natural frequency, assuming its invariance with respect to the vibration amplitude.

Modal Structural Damping

From the HT envelopes in air, a simple exponential fitting is used to assess the linear structural damping coefficient, as presented in Tab. 2.

Table 2 – Linear viscous damping for the first modal temporal free-decay series

	$\zeta_1\,(\%)$	
	Sinusoidal	**Bessel-like**
Air	0.49	0.49
Water	4.17	4.00

On the other hand, besides structural damping, the free decay in water is characterized by a nonlinear hydrodynamic dissipation, usually modeled quadratically by Morison's drag formula, see Eq. 2. It would then be much more complicated to isolate both dissipation mechanisms. For the sake of simplicity, an equivalent linear damping coefficient for the free-decay in water is considered, as shown in Tab. 2, after an exponential fitting on the signal amplitude envelope is done.

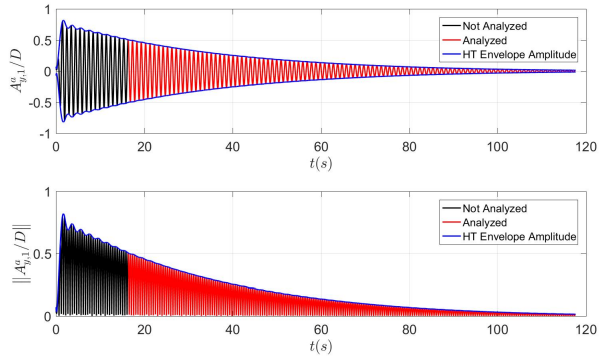

Figure 5 – Fundamental modal amplitude from sinusoidal decomposition: free-decay in air.

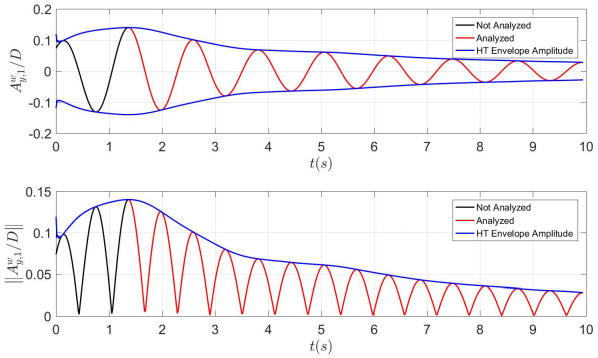

Figure 6 – Fundamental modal amplitude from sinusoidal decomposition: free-decay in water.

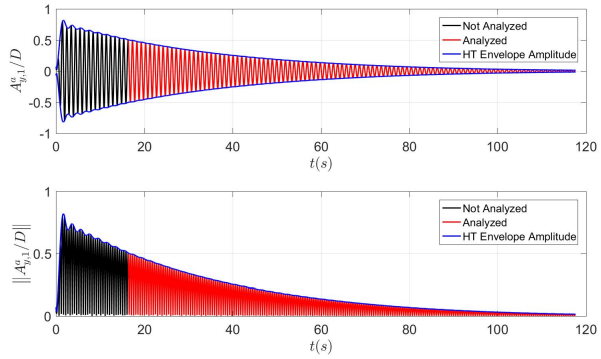

Figure 7 – Fundamental modal amplitude from Bessel-like decomposition: free-decay in air.

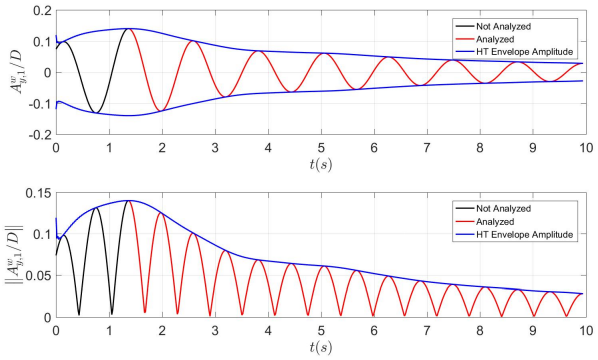

Figure 8 – Fundamental modal amplitude from Bessel-like decomposition: free-decay in water.

Instant frequency

The phase signal obtained from the Hilbert transform is used to determine the instant damped frequency of the free-decay experimental tests via numerical time differentiation. Figures 9–10 present the instant frequency determined for each free-decay test for both decompositions, sinusoidal and Bessel-like. The instant frequency is plotted as a function of the HT envelope normalized with respect to the diameter, in order to address its dependence on the vibration amplitude.

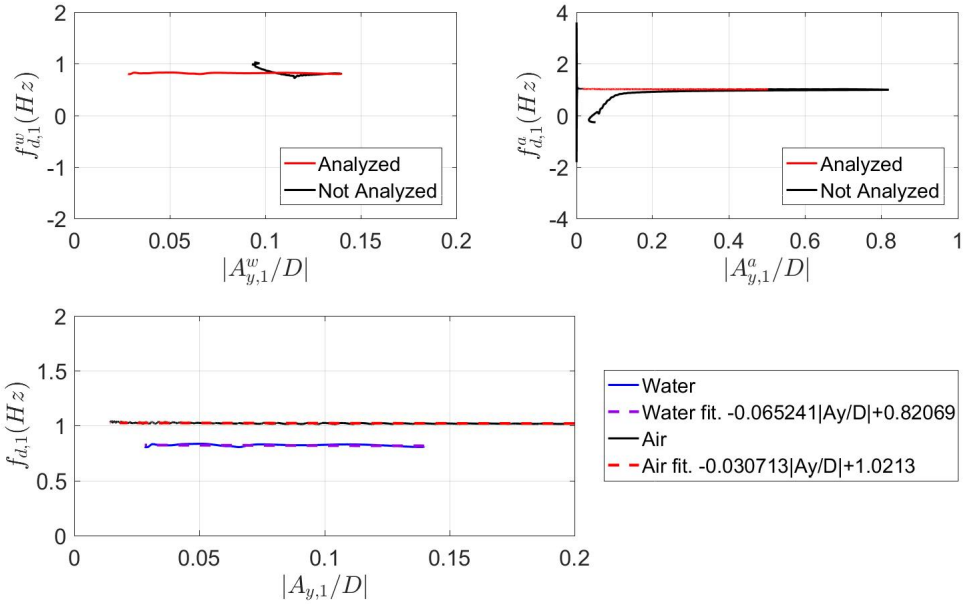

Figure 9 – Flexible vertical cylinder first mode instant damped frequency from free-decay tests in air and in water: sinusoidal basis.

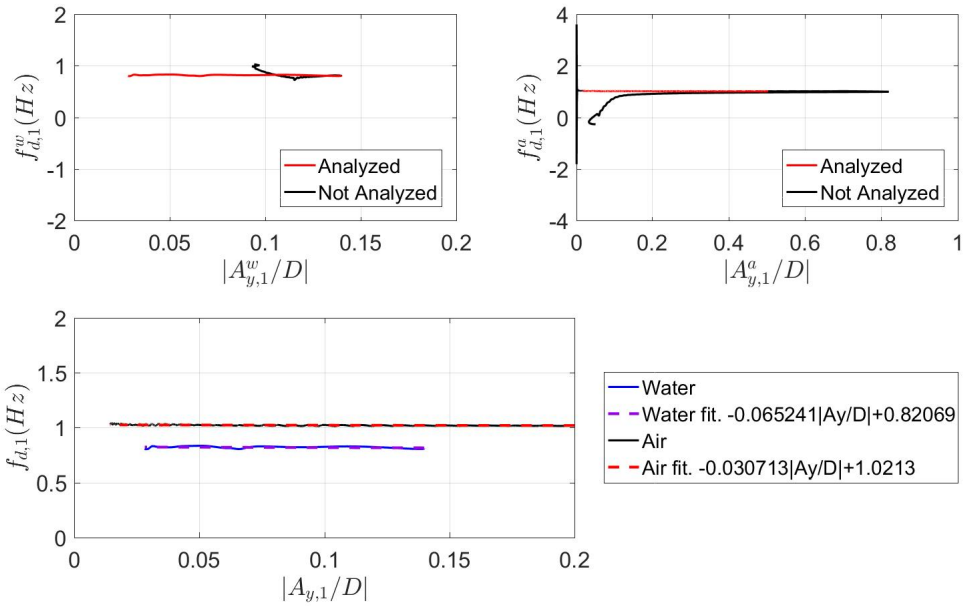

Figure 10 – Flexible vertical cylinder first mode instant damped frequency from free-decay tests in air and in water: Bessel-like basis.

Figures 9–10 also provides a linear fitting for the instant damped frequency calculated within the analysed vibration amplitude range. As it can be seen, the instant damped frequencies do not vary significantly with the vibration amplitude, being almost constant, either in air or water, irrespective the projection basis chosen.

Regarding both modal decompositions – Sinusoidal and Bessel-like – for the first mode amplitude, Table 3 shows the fundamental natural damped frequency measured using a standard Fourier analysis (FFT) and the results obtained with the HT instant frequency linear fittings presented in Figs. 9–10. Deviations between FFT and HT frequencies are also given, showing that both techniques meet equivalent results.

Table 3 – First mode natural damped frequencies, $f_{d,1}(Hz)$, measured with FFT and HT for both modal representations.

	Sinusoidal			Bessel-like		
	FFT	**HT**	**(FFT-HT)/FFT (%)**	**FFT**	**HT**	**(FFT-HT)/FFT (%)**
Air	1.0140	1.0213	−0.72	1.0140	1.0213	−0.72
Water	0.8211	0.8207	0.05	0.8211	0.8207	0.05

Added Mass Assessment

For the first mode, using modal mass and modal rigidity terms given in Eq. 4 and presented in Tab. 4, non damped frequencies, $\hat{f}_{n,1}$ as function of the first mode added mass coefficient, a_1, were calculated from Eqs. 5–6 and are given in Tab. 5 for both in water and in air. The damped natural frequencies, $f_{d,1}$, experimentally obtained from the FFT analysis, already presented in Tab 3, are reproduced in Tab. 5 for reference sake.

Table 4 – Modal mass and modal rigidity. First mode only. Sinusoidal and Bessel-like projections.

	Sinusoidal		Bessel-like	
	$\mathbf{M_1\,(kg)}$	$\eta_1\,(\mathbf{N/m})$	$\mathbf{M_1\,(kg)}$	$\eta_1\,(\mathbf{N/m})$
Air	1.5698	57.6515	1.2142	54.7226
Water	1.5482	56.8190	1.3083	52.8053

Table 5 – Damped natural frequencies from decay tests, using standard Fourier analysis (FFT), and non damped ones , having added mass coefficient as parameter.

	$\mathbf{f_{d,1}\,(Hz)}^{\dagger}$	$\mathbf{\hat{f}_{n,1}\sqrt{1+a_1}\,(Hz)}^{\ddagger}$	
		Sinusoidal	**Bessel-like**
Air	1.0140	0.9645	1.0685
Water	0.8211	0.9610	1.0112

†: Measured (FFT); ‡: Calculated.

Assume that the calculated natural damped frequency, $\hat{f}_{n,1}\sqrt{1-\zeta_1^2}$ (using the modal damping coefficient presented in Tab. 2 and the natural frequencies in Tab. 5), is a good estimate for the measured damped frequency, $f_{d,1}$. Then, by taking the ratio between the damped frequency, $f_{d,1}$, of both free-decay tests in air and in water, see Eq. 9, and recalling that the added mass in air is practically null, it is possible to assess the modal added mass coefficient in water, as given in Eq. 10.

$$\frac{f^a_{d,1}}{f^w_{d,1}} = \frac{\frac{\hat{f}^a_{n,1}\sqrt{1-\left(\zeta^a_1\right)^2}}{\sqrt{1+0}}}{\frac{\hat{f}^w_{n,1}\sqrt{1-\left(\zeta^w_1\right)^2}}{\sqrt{1+a_1}}} \approx \frac{\hat{f}^a_{n,1}}{\hat{f}^w_{n,1}}\sqrt{1+a_1},\ \text{as}\ \frac{\sqrt{1-\left(\zeta^a_1\right)^2}}{\sqrt{1-\left(\zeta^w_1\right)^2}} \approx 1 \tag{9}$$

$$a_1 = \left(\frac{\hat{f}^w_{n,1}}{\hat{f}^a_{n,1}}\frac{f^a_{d,1}}{f^w_{d,1}}\right)^2 - 1 \tag{10}$$

Defining a modal reduced mass parameter as the quotient between the modal structural mass and the modal displaced water mass, Eq. 11, the added mass coefficient related to the modal displaced mass, $C_{a,1}$, can be evaluated from the modal added mass coefficient related to the modal structural mass, a_1. In fact,

$$a_1 = \frac{M_{a,1}}{M_{s,1}} = \frac{M_{a,1}}{M_{d,1}}\frac{M_{d,1}}{M_{s,1}} = \frac{C_{a,1}}{m^\star_1},\ \text{in which}\ m^\star_1 = \frac{M_{s,1}}{M_{d,1}} = \frac{4m_s\int_0^L \psi_1^2(z)\,dz}{\pi\rho_w D^2\int_0^{L_i}\psi_1^2(z)\,dz} \tag{11}$$

$$C_{a,1} = m^\star_1 a_1 \tag{12}$$

Table 6 – Free-decay in water: modal integral numerical values for the modal oscillator mass term.

	Based on	
	Total length (L)	**Immersed length ($\mathbf{L_i}$)**
	$\mathbf{\int_0^L \psi_1^2(z)\,dz}\,(m)$	$\mathbf{\int_0^{L_i} \psi_1^2(z)\,dz}\,(m)$
Sinusoidal	1.3010	1.1285
Bessel-like	1.0994	1.0883

Using the modal integrals given in Tab. 6, two modal reduced mass parameters related to the model immersed length may be defined, as follows:

1. $m^{\star}_{I,1}$: model structure (as built) with length L and immersed length L_i;
2. $m^{\star}_{II,1}$: model structure hypothetically completely immersed, $L = L_i$.

The hypothetical case in which the structure would be completely immersed in the water, $m^{\star}_{II,1}$, is proposed in order to enforce some sort of similarity with the rigid circular cylinder studied in Sarpkaya (1977). The fact the model is or not completely immersed alters the modal reduced mass, inasmuch as the quantity of modal displaced mass also changes.

Table 7 shows the values of the modal reduced mass for both cases defined before and both modal shapes considered. Along with the modal reduced mass, the modal added mass related to the displaced mass is also calculated. The Bessel-like modal shape is physically closer to the actual modal shape and, as Tab. 7 shows, choosing the modal representation affects the modal added mass coefficient substantially.

Table 7 – First mode added-mass coefficients – a_1 and $C_{a,1}$ – and corresponding mass-ratios. $a_1 = m_{a,1}/m_{s,1}$ determined from Eq. 10, with damped natural frequencies obtained from standard Fourier analysis.

		$\mathbf{L_i < L}$		$\mathbf{L_i = L}$	
	$\mathbf{a_1}$	$\mathbf{m^{\star}_{I}}$	$\mathbf{C^{I}_{a,1}}$	$\mathbf{m^{\star}_{II}}$	$\mathbf{C^{II}_{a,1}}$
Sinusoidal	0.514	3.455	1.776	2.997	1.541
Bessel-like	0.387	3.028	1.172	2.997	1.160

Although the modal added mass result obtained using the Bessel-like mode is around 17% larger than the 'potential-flow' one, $\hat{C}_{a,1} \approx 1$, the same asymptotic behavior ($C_a \to 1^+$ for low KC, in the present experiment of order 1) as in the rigid cylinder case studied by Sarpkaya (1977) is observed; see Fig. 2 and regard the logarithm scale used. It should be noticed that, by using essentially the same methodology, with a proper *eigenmode* for a cantilevered flexible circular cylinder, Pesce and Fujarra (2000) had experimentally obtained the first modal added mass coefficient $C_{a,1} = 1.17$, in a remarkable agreement with the present assessment.

Figures 11–12b present the modal added mass parameters, a_1 and $C_{a,1}$, as function of the HT envelope amplitude obtained using the instant damped frequency linear fittings determined in Figs. 9–10. The values found using the HT methodology at zero amplitude meet the outcomes presented in Tab. 7 with a standard Fourier analysis. Notice that the quadratic form for a_1, as per Eq. 10, increases the differences found in the damped natural frequencies, if HT or FFT analysis are used, (compare Figs. 9–10 and Tab. 3).

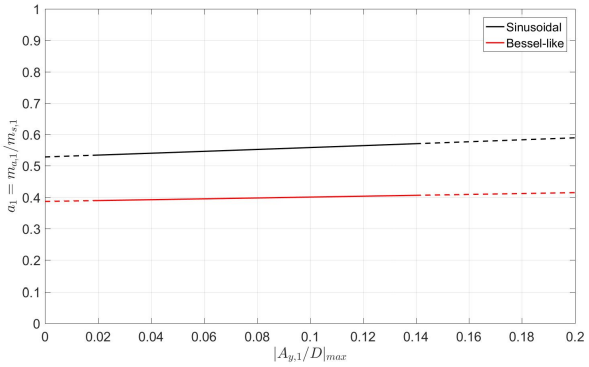

Figure 11 – Added mass coefficient, a_1, with respect to the structural mass, for the first mode, as function of the HT envelope amplitude for sinusoidal and Bessel-like modal projections.

Finally, Figure 12a shows the first mode added mass coefficient, determined with respect to the modal displaced mass, $m^{\star}_{I,1}$, which is based on the as built immersed length. On the other hand, Figure 12b uses the hypothetical case in which the structure is considered completely immersed in the water.

Comparing Figures 12a–b, it can be readily noticed that the way the modal reduced mass is defined does not affect significantly the results. However, the way the decomposition basis is taken, has indeed a significant effect. Moreover, if the Bessel-like projection is taken, the simple and standard Fourier analysis procedure leads to results which are in remarkable agreement with that reported by Pesce and Fujarra (2000) for a cantilevered flexible cylinder, $C_{a,1} = 1.17$. As a matter of fact, such a value is less than 20% larger than $\hat{C}_{a,1} = 1$, the small amplitude added mass value that should be expected from a presumed rigid cylinder similarity.

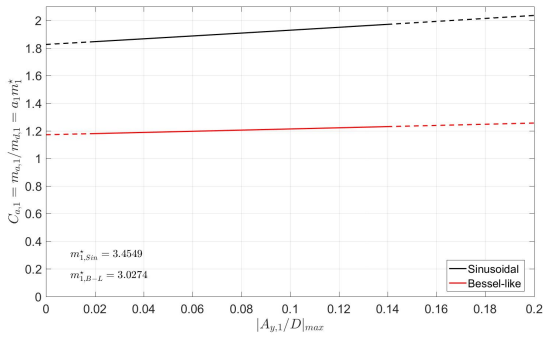

(a) Added mass, $C_{a,1}$, with respect to the as built displaced mass.

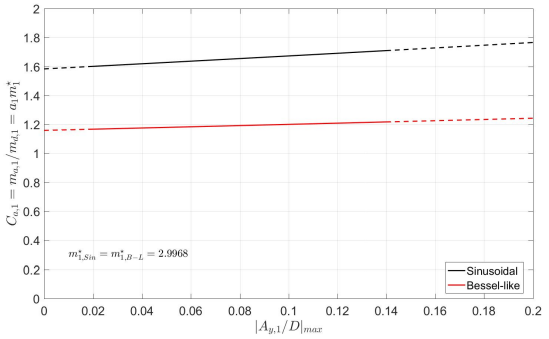

(b) Added mass, $C_{a,1}$, with respect to an hypothetical full-length displaced mass.

Figure 12 – Added mass coefficient, $C_{a,1}$, for the first mode, as function of the HT envelope amplitude for sinusoidal and Bessel-like modal projections.

CONCLUSIONS

A modal added mass coefficient assessment using two free-decay experimental tests for the same model, in immersed and non-immersed conditions, was successfully carried out using standard (Fourier) and non-standard (Hilbert Transform) analysis methodologies. Applying usual Galerkin's projection schemes, the first mode added mass coefficient was assessed, by using two distinct trial functions basis: the simplest one – sinusoidal; and a Bessel-like eigenfunction set, arisen from an accurate asymptotic modeling regarding the vertical tensioned beam dynamic problem. The choice of a sufficiently representative modal shape has shown to be essential, altering significantly the experimental assessment of the first mode added mass coefficient, for a vertical flexible cylinder configuration. Along with the choice of a representation basis, the modal added mass, due to a quadratically form, presents a significant numerical sensitivity for small deviations in the frequency values obtained using FFT or HT methodologies.

The present experimental assessment for the first mode added mass of a vertical flexible circular cylinder fixed at both extremities showed a remarkable agreement with that reported by Pesce and Fujarra (2000) for a cantilevered one, $C_{a,1} = 1.17$. This value is just 17% larger than the potential flow added mass coefficient, $\hat{C}_a = 1$, commonly assumed in riser engineering, in an *ad-hoc* manner. It should be also noticed that the well-known experimental chart by Sarpkaya (1977), for rigid cylinders in oscillatory flow, shows - in log scale - an asymptotic limit for the inertia coefficient, $C_m = 1 + C_a$, slightly larger than 2.

The next step for the modal added mass coefficient assessment would be expanding the analysis for higher modes, looking for a wider scenario involving the evaluation of added mass parameters for Reduced Order Models. The Hilbert Transform methodology is also an asset of the present work, being possible to use it in other experimental tests to determine the dependency of the system natural frequency on the vibration amplitude. A subsidiary and practical result, emerged during the HT methodology application, is the possibility of an *a posteriori* assessment of the optical tracking system measurement, being it in air or water, as shown in the Appendix.

ACKNOWLEDGMENTS

The results presented in the paper were obtained from a comprehensive research project on non-linear dynamics of risers sponsored by Petrobras and carried out in 2011–2013. The Coordination for the Improvement of Higher Education Personnel, CAPES, is acknowledged by the first author for the PhD grant 33002010049-P9. The National Council for Scientific and Technological Development, CNPq, is acknowledged by the second author for the research grant 308990/2014-5. Special thanks to Drs. Guilherme Franzini, Rodolfo Gonçalves and to the IPT towing tank technical staff.

REFERENCES

Franzini, G.R.; Pesce, C.P.; Salles, R.; Gonçalves, R.T.; Fujarra, A.L.C.; Mendes, P., 2015. "Experimental Analysis of a Vertical and Flexible Cylinder in Water: Response to Top Motion Excitation and Parametric Resonance". Journal of Vibration and Acoustics, Vol. 137. doi: 10.1115/1.4025759.

Franzini, G.R.; Pesce, C.P.; Gonçalves, R.T.; Fujarra, A.L.C.; Mendes, P., 2016. "Experimental Investigations on Vortex-Induced Vibrations with a Long Flexible Cylinder. Part I: Modal-Amplitude Analysis with a Vertical Configuration". FIV.

Franzini, G.R.; Pesce, C.P.; Gonçalves, R.T.; Fujarra, A.L.C.; Mendes, P., 2016. "Experimental Investigations on Vortex-Induced Vibrations with a Long Flexible Cylinder. Part II: Effect of Axial Motion Excitation in a Vertical Configuration". FIV.

Franzini, G.R.; Santos, C.C.P.; Pesce, C.P.; Mazzilli, C.E.N., 2016. "Parametric Excitation of an Immersed, Vertical and Slender Beam using Reduced-Order Models: Influence of Hydrodynamic Coefficients". Marine Systems and

Ocean Technology. doi: 10.1007/s40868-016-0013-z.
Fu, S.; Wang, J.; Baarholm, R.; Wu, J.; Larsen, C.M., 2014. "Features of Vortex-Induced Vibration in Oscillatory Flow". ASME, J. Offshore Mech. Arct. Eng. 136(1):011801–011801.
Kuiper, G.L., 2008, "Stability of Offshore Risers Conveying Fluid", Eburon.
Mazzilli, C.E.N.; Lenci, S.; Demeio, L., 2014. "Nonlinear free vibrations of tensioned vertical risers". In Proceedings of the 8th European Nonlinear Dynamics Conference (ENOC2014).
Morooka, C.K.; Tsukada, R.I., 2013. "Experiments with a Steel Catenary Riser Model in a Towing Tank". Applied Ocean Research, v. 43, 244-255.
Pereira, F.R., 2014. "Investigação das Vibrações Induzidas pela Emissão de Vórtices em Modelos Reduzidos de Riser Lançados em Catenária". PhD. Thesis, Escola Politécnica, Universidade de São Paulo, São Paulo, Brasil.
Pereira, F.R.; Pesce, C.P.; Gonçalves, R.T.; Franzini, G.R.; Fujarra, A.L.C.; Salles, R.; Mendes, P., 2012. "Risers Model Test: Scaling Methodology and Dynamic Similarity". Proceedings of the 22nd International Society of Offshore and Polar Engineers (ISOPE2012).
Pereira, F.R.; Pesce, C.P.; Gonçalves, R.T.; Fujarra, A.L.C.; Franzini, G.R.; Mendes, P., 2016. "Experimental Investigations on Vortex-Induced Vibrations with a Long Flexible Cylinder. Part III: Modal-Amplitude Analysis with a Catenary Configuration". FIV.
Pesce, C.P., 2013. "Riser dynamics: experiments with small scale models". LabOceano - Ten-Years Anniversary Celebration Workshop, April 29-30.
Pesce, C.P.; and Fujarra, A.L.C., 2000. "Vortexinduced vibrations and jump phenomenon: Experiments with a clamped flexible cylinder in water". International Journal of Offshore and Polar Engineering, 10, pp. 26–33.
Pesce, C.P.; Fujarra, A.L.C.; Simos, A.N.; Tanuri, E.A., 1999. "Analytical and closed-form solution for deep water riser-like eigenvalue problem". Proceedings of the 9th International Ocean and Polar Engineering Conference (ISOPE).
Salles, R., 2016, "Experimental Analysis of Fluid-Structure Interaction Phenomena on a Vertical Flexible Cylinder: Modal Coefficients and Parametric Resonance", Master's Thesis, Escola Politécnica da Universidade de São Paulo, São Paulo, Brazil.
Sarpkaya, T., 1977, "In-Line and Transverse Forces on Cylinders in Oscillatory Flow at High Reynolds Number". Journal of Ship Research, 200–2016. doi: 10.1016/0167-2789(83)90298-1.
Thorsen, M.J.; Saevik, S.; Larsen, C.M., 2016. "Time domain simulation of vortex-induced vibrations in stationary and oscillating flows". Journal of Fluids and Structures 61, pp. 1–19. doi: 10.1016/j.jfluidstructs.2015.11.006.

APPENDIX – THE HT METHODOLOGY AS A TOOL TO ASSESS OPTICAL TRACKING ACCURACY

During the experimental set up in air and water, the calibration of the optical tracking system revealed a measurement accuracy about a decimal of millimeter ($0.1mm$). On the other hand, by using the HT procedure to evaluate the instant damped frequency as function of vibration amplitude, resolution is clearly obtained, revealing a figure better than $0.005 \times D = 0.005 \times 22.2mm \approx 0.1mm$, as shows Fig. 13, for the decay test in air.

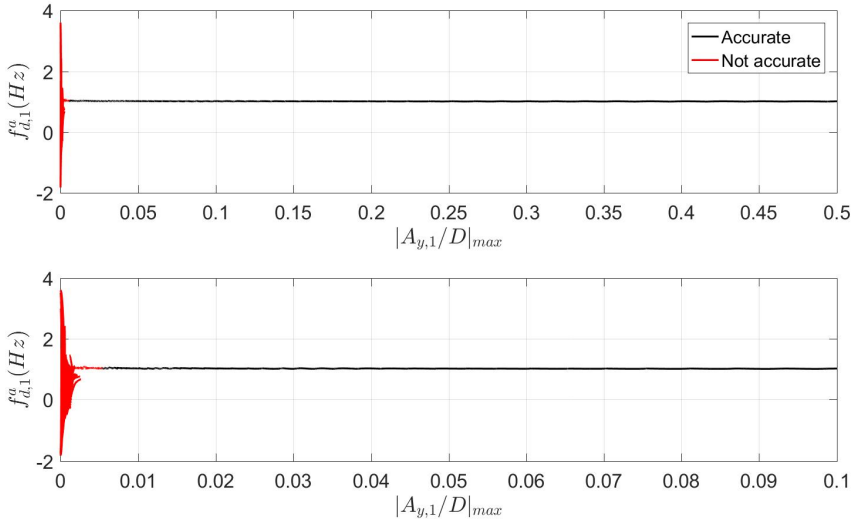

Figure 13 – Instant damped frequency from free-decay in air showing a clear bound for the optical tracking system accuracy.

RESPONSIBILITY NOTICE

The authors are the only responsible for the material included in this paper.